Electronic Supplementary Information

Cadmium-rich intermetallic phases ARh$_2$Cd$_{20}$ – Structure, magnetic behavior, ^{151}Eu Mössbauer and ^{113}Cd solid-state NMR spectroscopy

Lars Schumacher[a], Florian Schreiner[b], Aylin Koldemir[a], Oliver Janka[c], Michael Ryan Hansen[b] and Rainer Pöttgen*[a]

[a] *Institut für Anorganische und Analytische Chemie, Universität Münster, Corrensstraße 30, 48149 Münster, Germany. E-mail: pottgen@uni-muenster.de*

[b] *Institut für Physikalische Chemie, Universität Münster, Corrensstrasse 30, D-48149 Münster, Germany*

[c] *Universität des Saarlandes, Anorganische Festkörperchemie, Campus C4 1, 66123 Saarbrücken, Germany*

ORCID:

Lars Schumacher	0009-0009-9444-8773
Florian Schreiner	0009-0007-4486-7940
Michael Ryan Hansen	0000-0001-7114-8051
Aylin Koldemir	0009-0004-3819-3853
Oliver Janka	0000-0002-9480-3888
Rainer Pöttgen	0000-0003-0962-279X

Received ## December 2024, Accepted ## ####### 2025

DOI: ########

Table S1 Experimental parameters for the static WCPMG and WCPMG-MAS NMR experiments.[a]

Sample	Nucleus	τ / µs	Ω / MHz	N	NS	d_1 / s	ν_{MAS} / kHz	n_{rot}	Echoes recorded	Echoes processed
YRh_2Cd_{20}	^{89}Y	150	0.5	80	512	32.0	–	–	128	64
	^{103}Rh	500	0.4	80	32768	2.0	–	–	80	80
	^{113}Cd	50	0.5	80	2048	8.0	12.5	9	80	12
$LaRh_2Cd_{20}$	^{103}Rh	500	0.4	80	32768	2.0	–	–	80	80
	^{113}Cd	50	0.5	80	32768	2.0	10.0	7	80	12
	^{113}Cd	50	0.5	80	8192	8.0	12.5	7	80	12
$YbRh_2Cd_{20}$	^{171}Yb	50	1.0	40	10240	6.0	–	–	80	20
	^{103}Rh	500	0.4	80	32768	2.0	–	–	80	80
	^{113}Cd	50	0.5	80	2048	8.0	12.5	9	80	12

[a] The listed parameters correspond to: pulse length τ, WURST sweep width Ω, WURST shape parameter N, number of scans NS, recycle delay d_1, number of acquired echoes as well as number of processed echoes, and in the case of WCPMG-MAS experiments, MAS frequency ν_{MAS} and number of rotor periods recorded per echo n_{rot}.

Table S2 Lattice parameters and mass% of $LaRh_2Cd_{20}$ and $RhCd_{9+\delta}$ for the first and second measurement. Standard deviations are given in parentheses.

Compound	a (pm)	V (nm^3)	mass%
first measurement			
$LaRh_2Cd_{20}$	1565.22(1)	3.8350	69.3(2)
$RhCd_{9+\delta}$	2008.88(4)	8.1071	30.7(2)
second measurement			
$LaRh_2Cd_{20}$	1565.27(1)	3.8350	60.1(2)
$RhCd_{9+\delta}$	2008.57(2)	8.1033	39.9(2)

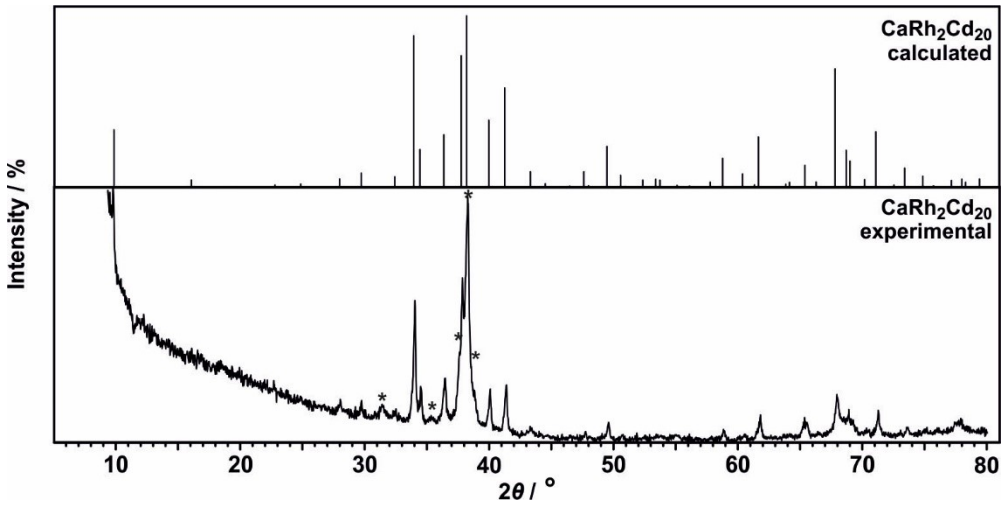

Fig. S1 Calculated (top) and experimental (bottom) Guinier powder patterns (Cu$K\alpha_1$ radiation) of the $CaRh_2Cd_{20}$ sample. Asterisks mark reflections from side-products.

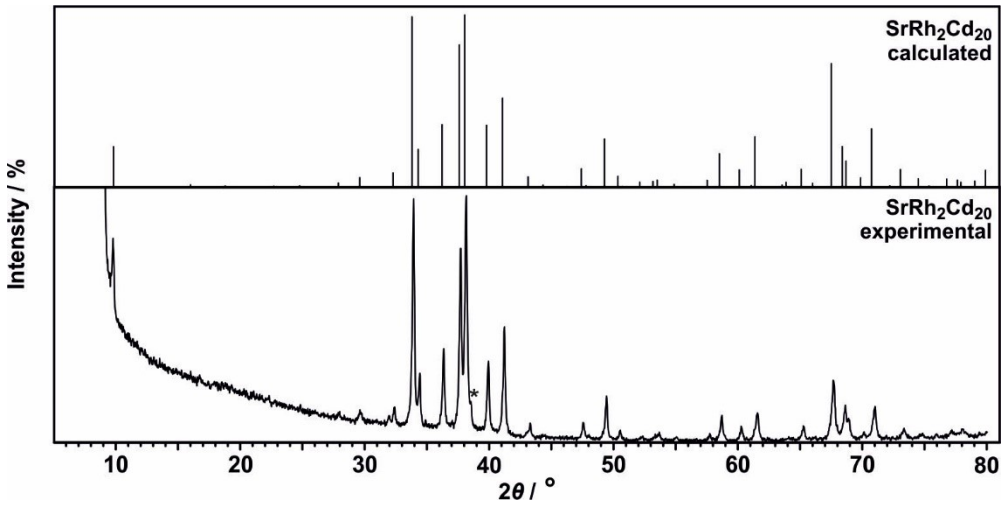

Fig. S2 Calculated (top) and experimental (bottom) Guinier powder patterns (Cu$K\alpha_1$ radiation) of the $SrRh_2Cd_{20}$ sample. Asterisks mark reflections from side-products.

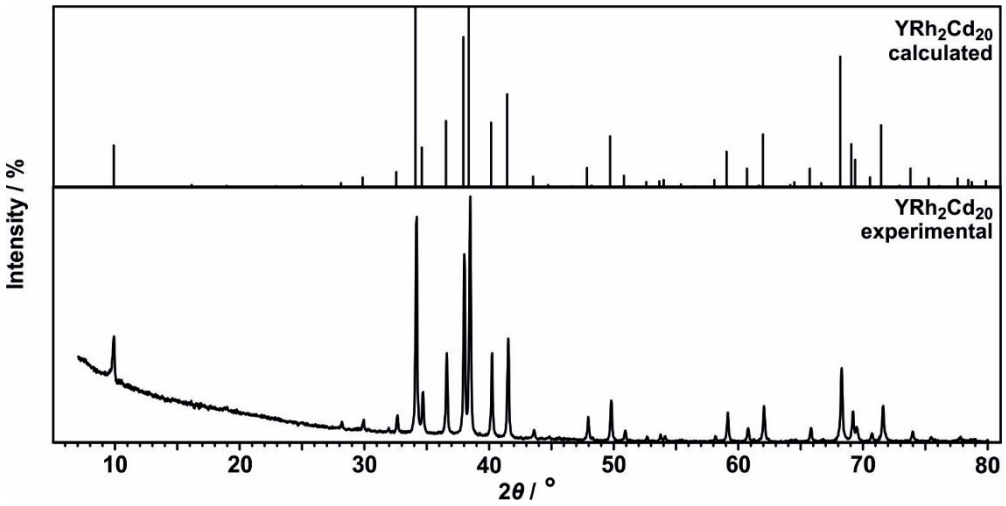

Fig. S3 Calculated (top) and experimental (bottom) Guinier powder patterns (Cu$K\alpha_1$ radiation) of the YRh_2Cd_{20} sample.

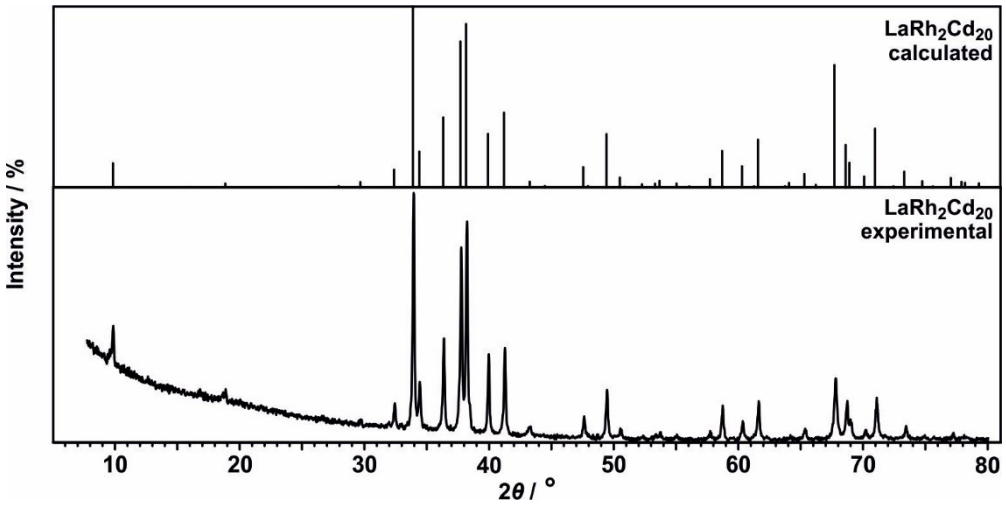

Fig. S4 Calculated (top) and experimental (bottom) Guinier powder patterns (Cu$K\alpha_1$ radiation) of the $LaRh_2Cd_{20}$ sample.

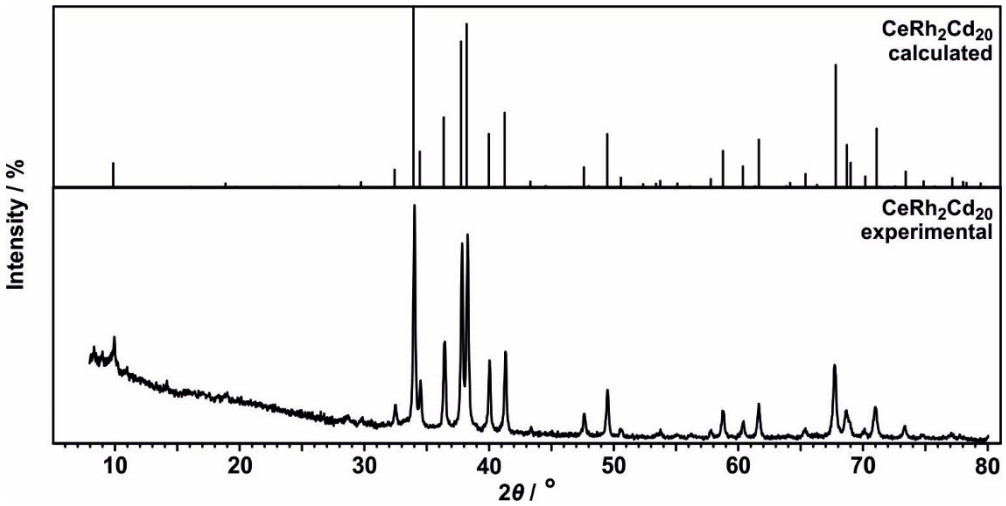

Fig. S5 Calculated (top) and experimental (bottom) Guinier powder patterns (Cu$K\alpha_1$ radiation) of the $CeRh_2Cd_{20}$ sample.

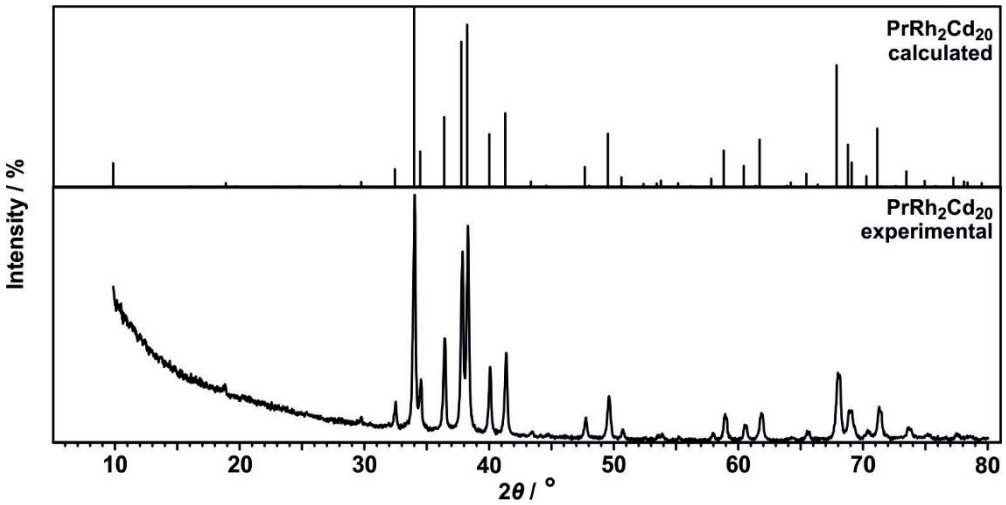

Fig. S6 Calculated (top) and experimental (bottom) Guinier powder patterns (Cu$K\alpha_1$ radiation) of the $PrRh_2Cd_{20}$ sample.

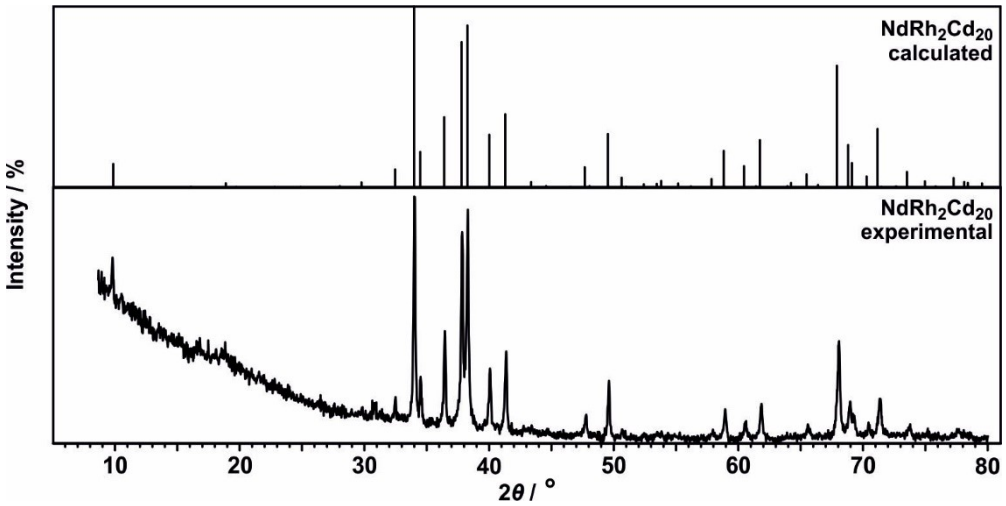

Fig. S7 Calculated (top) and experimental (bottom) Guinier powder patterns (Cu$K\alpha_1$ radiation) of the $NdRh_2Cd_{20}$ sample.

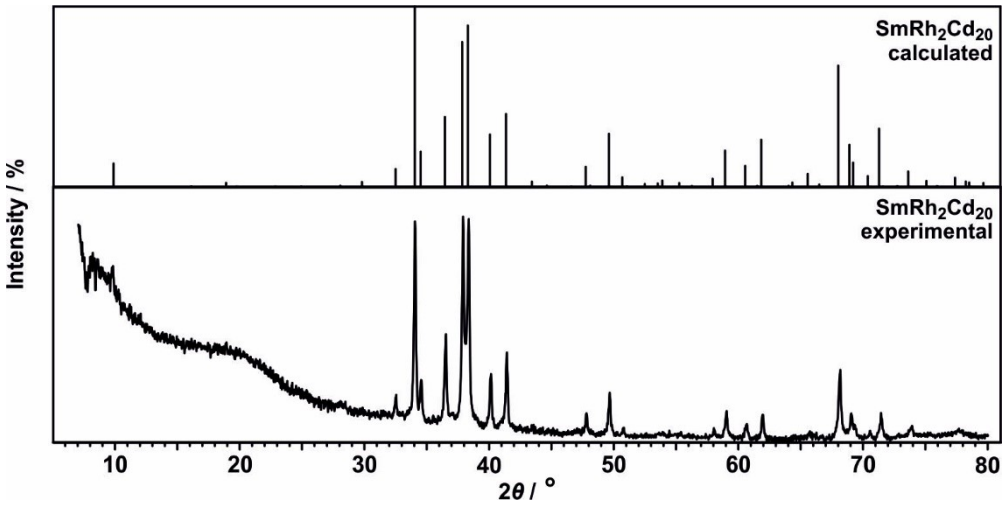

Fig. S8 Calculated (top) and experimental (bottom) Guinier powder patterns (Cu$K\alpha_1$ radiation) of the $SmRh_2Cd_{20}$ sample.

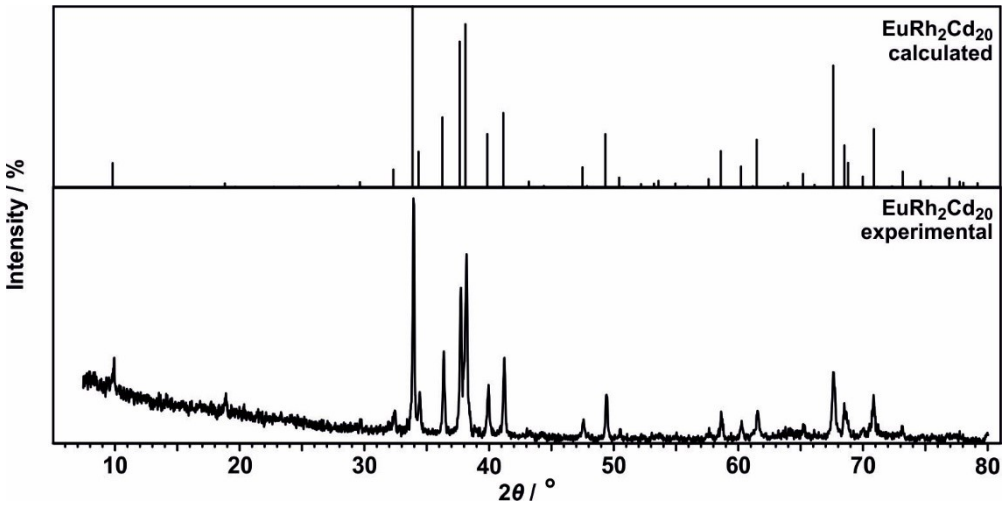

Fig. S9 Calculated (top) and experimental (bottom) Guinier powder patterns (Cu$K\alpha_1$ radiation) of the $EuRh_2Cd_{20}$ sample.

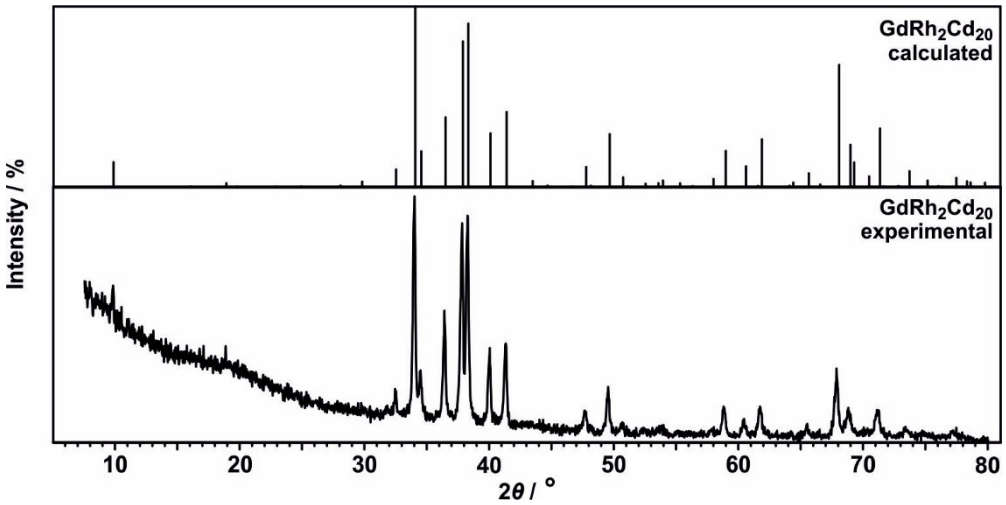

Fig. S10 Calculated (top) and experimental (bottom) Guinier powder patterns (Cu$K\alpha_1$ radiation) of the $GdRh_2Cd_{20}$ sample.

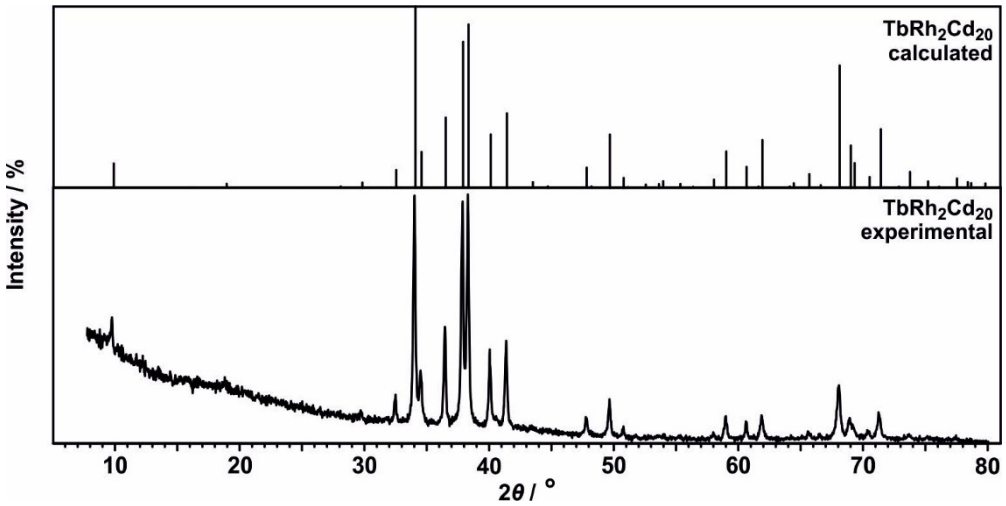

Fig. S11 Calculated (top) and experimental (bottom) Guinier powder patterns (Cu$K\alpha_1$ radiation) of the $TbRh_2Cd_{20}$ sample.

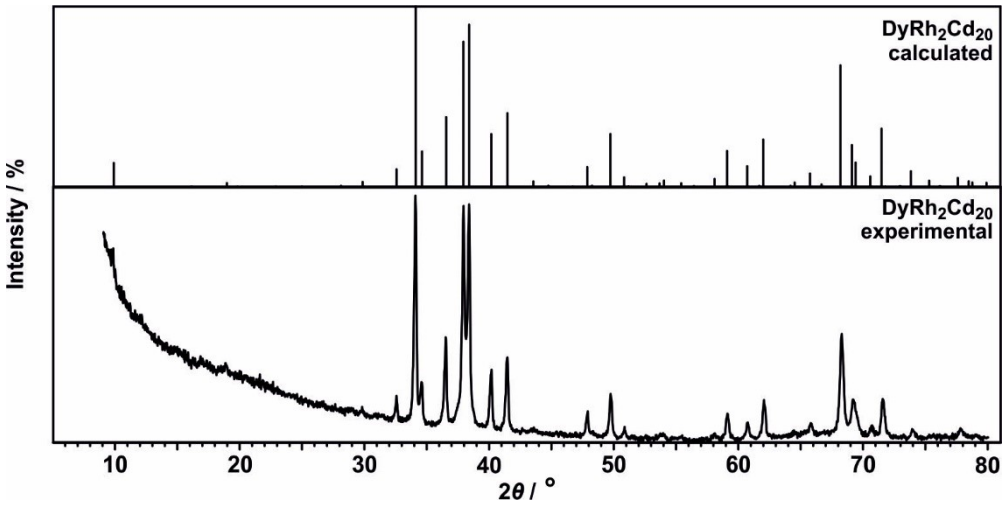

Fig. S12 Calculated (top) and experimental (bottom) Guinier powder patterns (Cu$K\alpha_1$ radiation) of the $DyRh_2Cd_{20}$ sample.

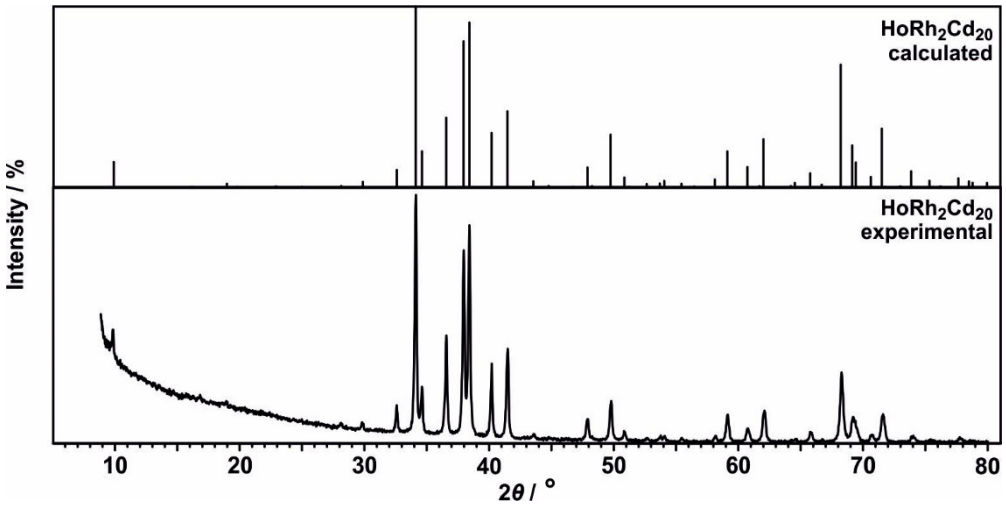

Fig. S13 Calculated (top) and experimental (bottom) Guinier powder patterns (Cu$K\alpha_1$ radiation) of the $HoRh_2Cd_{20}$ sample.

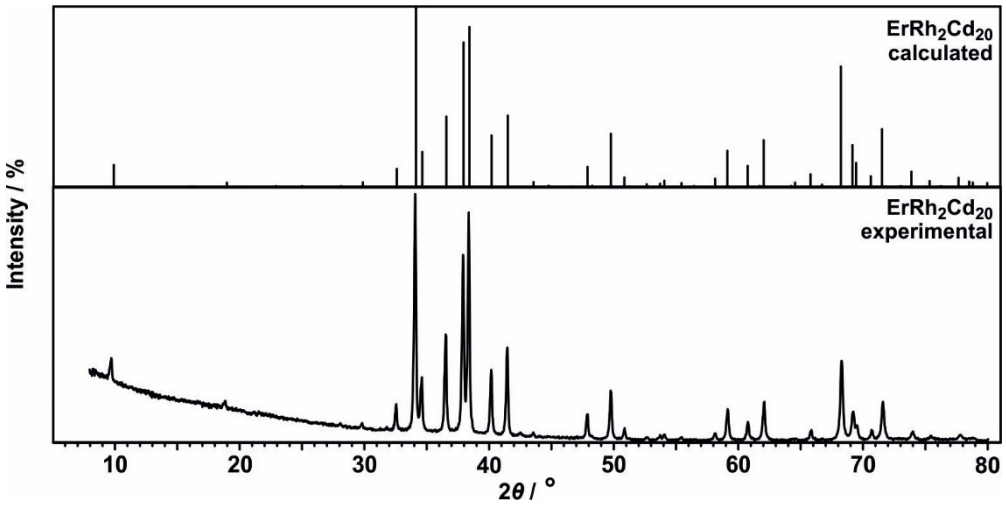

Fig. S14 Calculated (top) and experimental (bottom) Guinier powder patterns (Cu$K\alpha_1$ radiation) of the $ErRh_2Cd_{20}$ sample.

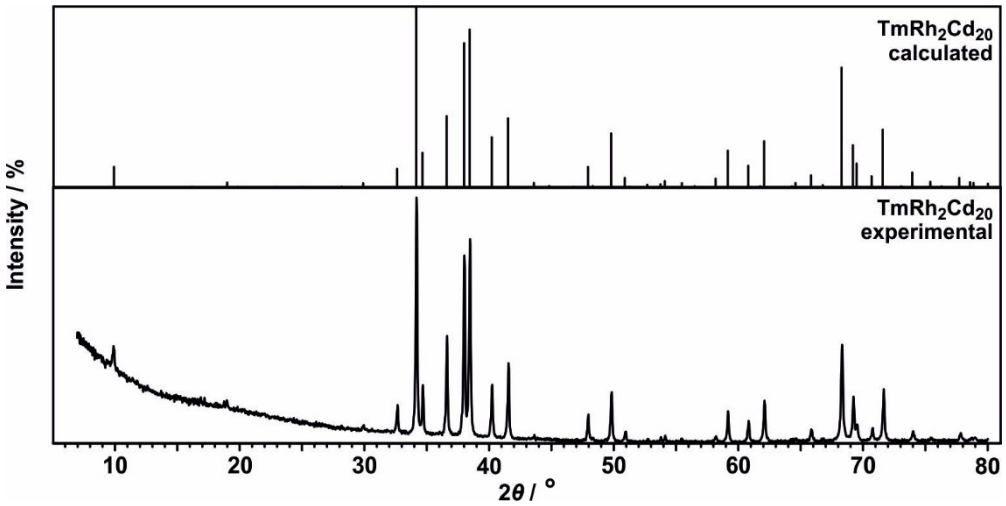

Fig. S15 Calculated (top) and experimental (bottom) Guinier powder patterns (Cu$K\alpha_1$ radiation) of the $TmRh_2Cd_{20}$ sample.

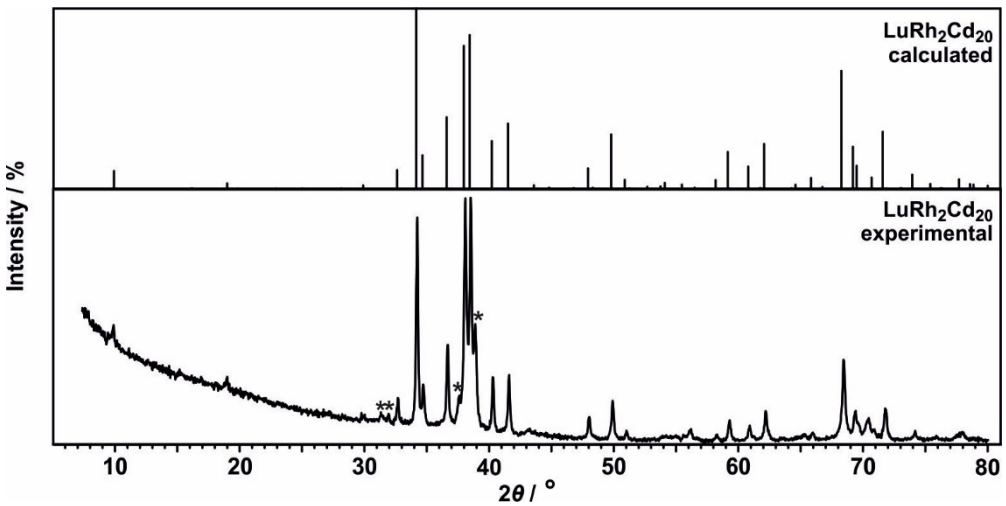

Fig. S16 Calculated (top) and experimental (bottom) Guinier powder patterns (Cu$K\alpha_1$ radiation) of the $LuRh_2Cd_{20}$ sample. Asterisks mark reflections from side-products.

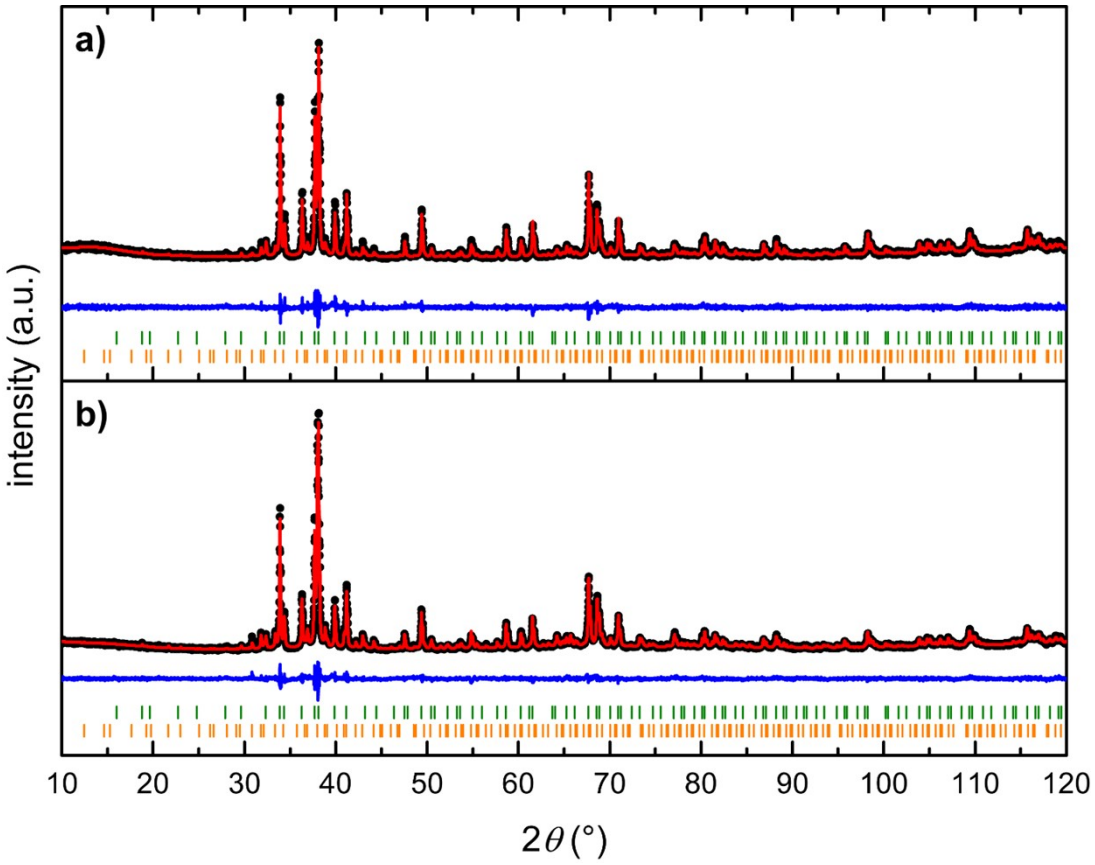

Fig. S17 Rietveld refinements of $LaRh_2Cd_{20}$. (a) After approximately 4 weeks after preparation and (b) three weeks after recording the diffraction pattern shown in (a). Black points: experimental data, red line: refined pattern, blue line: difference experimental minus refined. Green dashes indicate the Bragg positions of $LaRh_2Cd_{20}$, orange dashes the ones of $RhCd_{9+\delta}$.

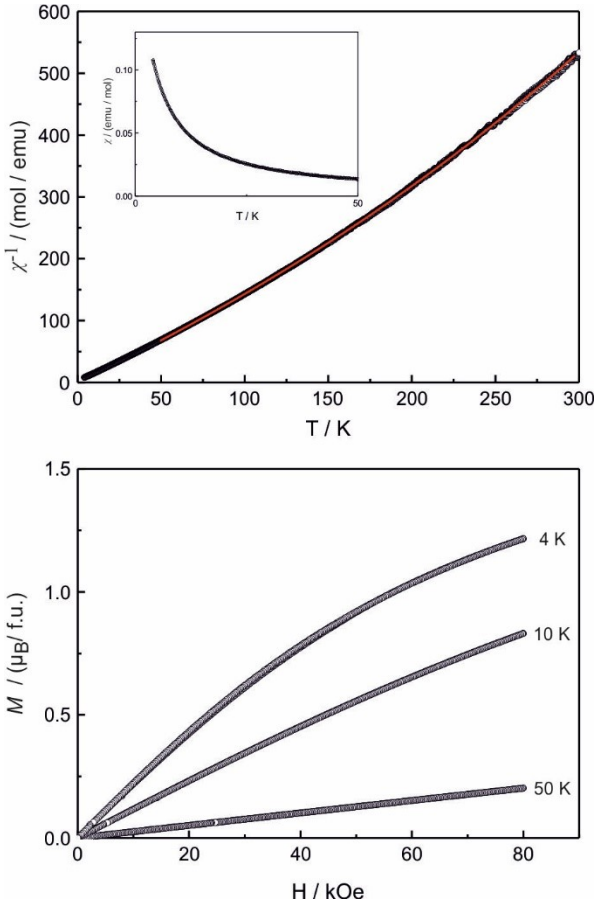

Figure S18 Magnetic data of $CeRh_2Cd_{20}$: Zero field cooled / field cooled (ZFC/FC) measurements at an applied field of 100 Oe (inset), inverse susceptibilities measured at 10 kOe; the red line emphasizes the fit regime (top) and magnetization isotherms recorded at 4, 10 and 50 K.

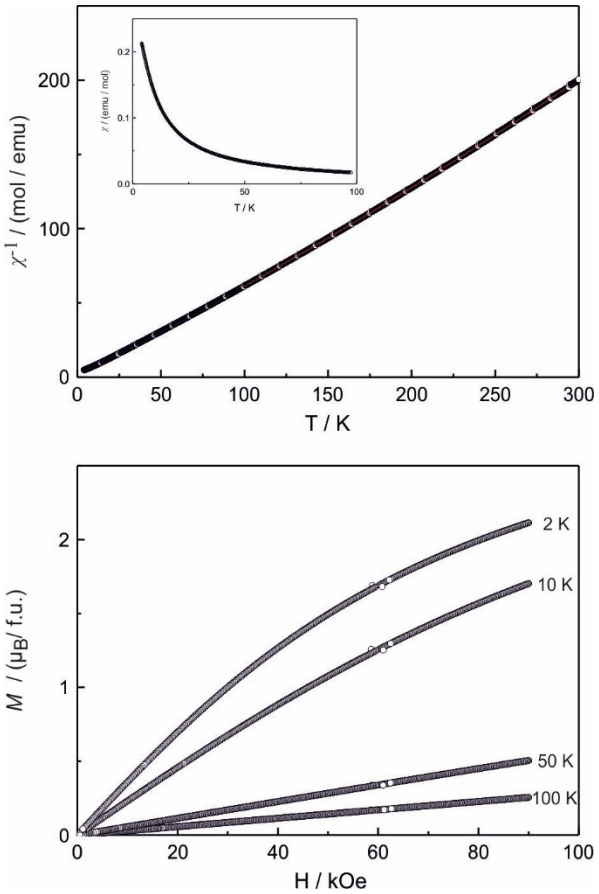

Figure S19 Magnetic data of $PrRh_2Cd_{20}$: Zero field cooled / field cooled (ZFC/FC) measurements at an applied field of 100 Oe (inset), inverse susceptibilities measured at 10 kOe (top) and magnetization isotherms recorded at 2, 10, 50 and 100 K.

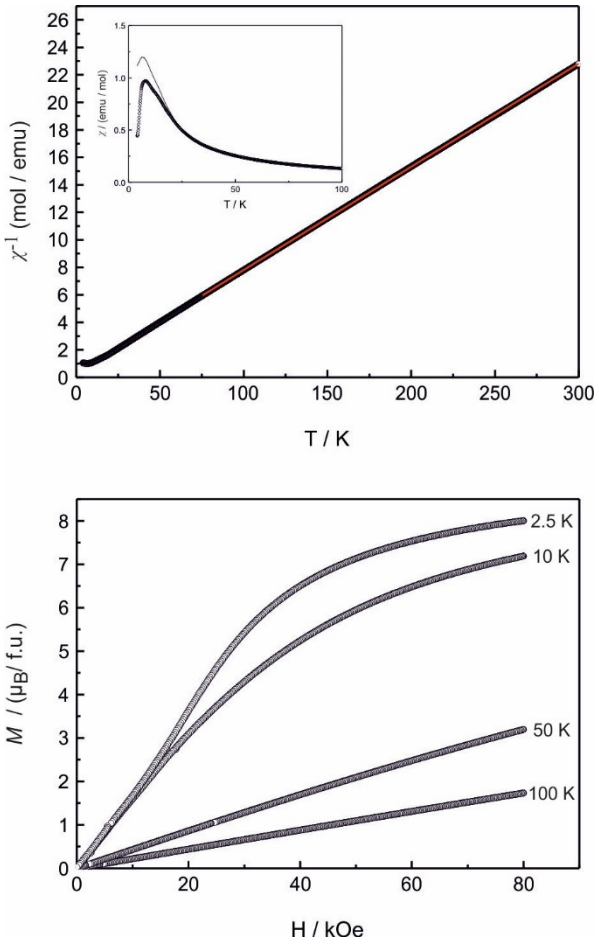

Figure S20 Magnetic data of $TbRh_2Cd_{20}$: Zero field cooled / field cooled (ZFC/FC) measurements at an applied field of 100 Oe (inset), inverse susceptibilities measured at 10 kOe; the red line emphasizes the fit regime (top) and magnetization isotherms recorded at 2.5, 10, 50 and 100 K.

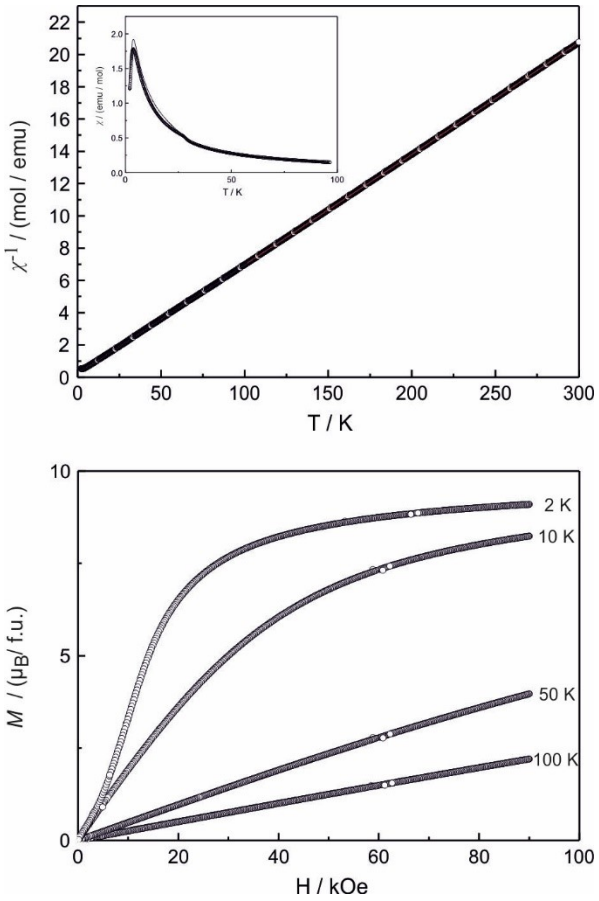

Figure S21 Magnetic data of $DyRh_2Cd_{20}$: Zero field cooled / field cooled (ZFC/FC) measurements at an applied field of 100 Oe (inset), inverse susceptibilities measured at 10 kOe (top) and magnetization isotherms recorded at 2, 10, 50 and 100 K.

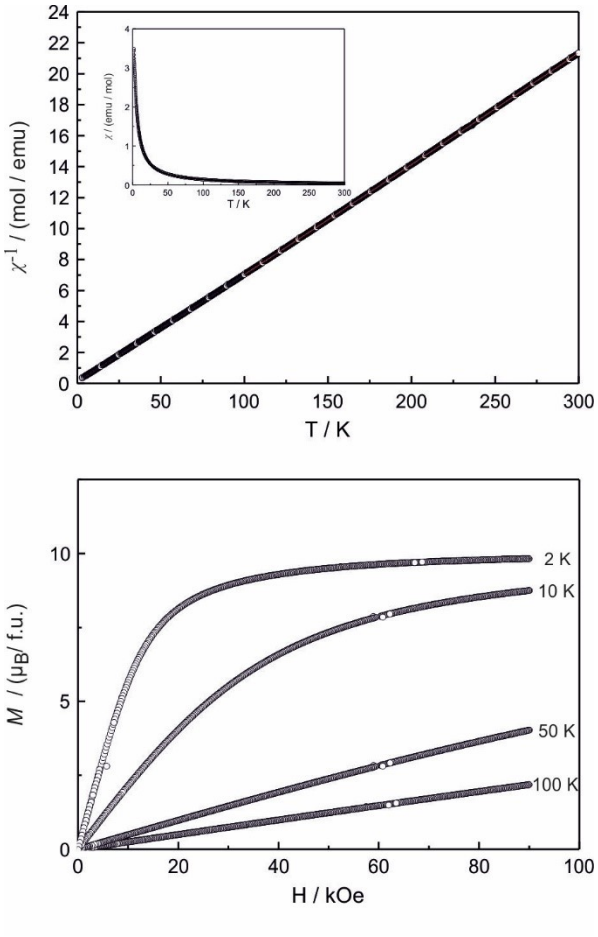

Figure S22 Magnetic data of $HoRh_2Cd_{20}$: Zero field cooled / field cooled (ZFC/FC) measurements at an applied field of 100 Oe (inset), inverse susceptibilities measured at 10 kOe (top) and magnetization isotherms recorded at 2, 10, 50 and 100 K.

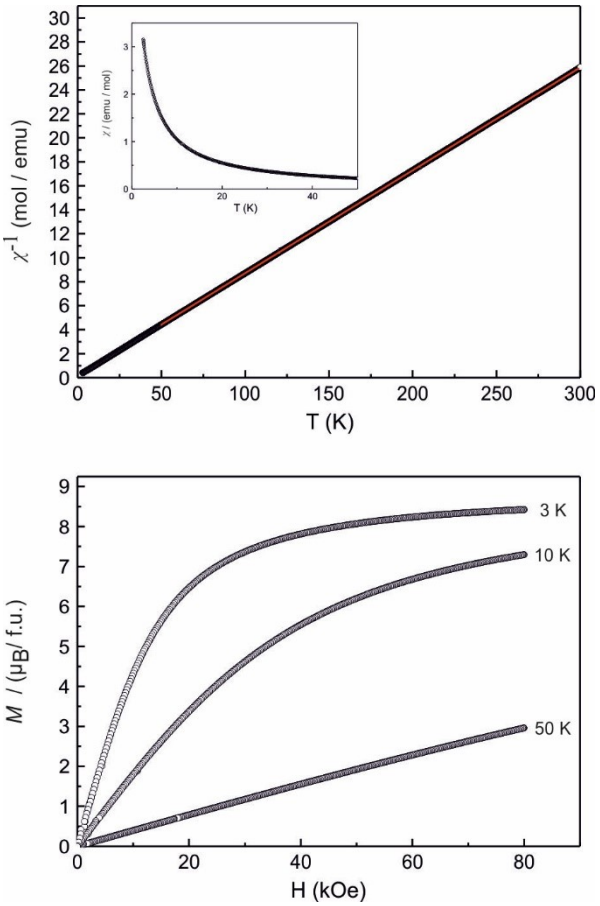

Figure S23 Magnetic data of $ErRh_2Cd_{20}$: Zero field cooled / field cooled (ZFC/FC) measurements at an applied field of 100 Oe (inset), inverse susceptibilities measured at 10 kOe; the red line emphasizes the fit regime (top) and magnetization isotherms recorded at 3, 10 and 50 K.

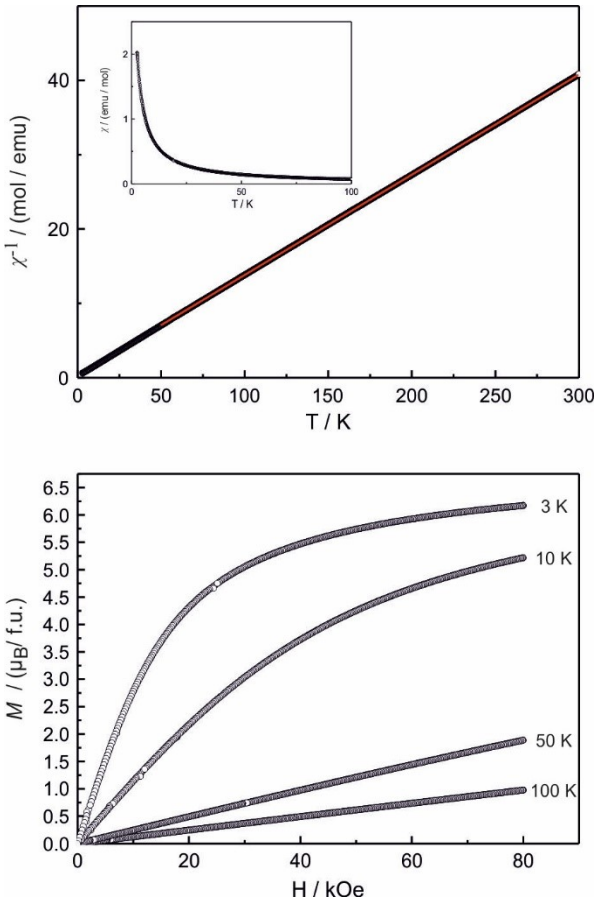

Figure S24 Magnetic data of $TmRh_2Cd_{20}$: Zero field cooled / field cooled (ZFC/FC) measurements at an applied field of 100 Oe (inset), inverse susceptibilities measured at 10 kOe; the red line emphasizes the fit regime (top) and magnetization isotherms recorded at 3, 10, 50 and 100 K.

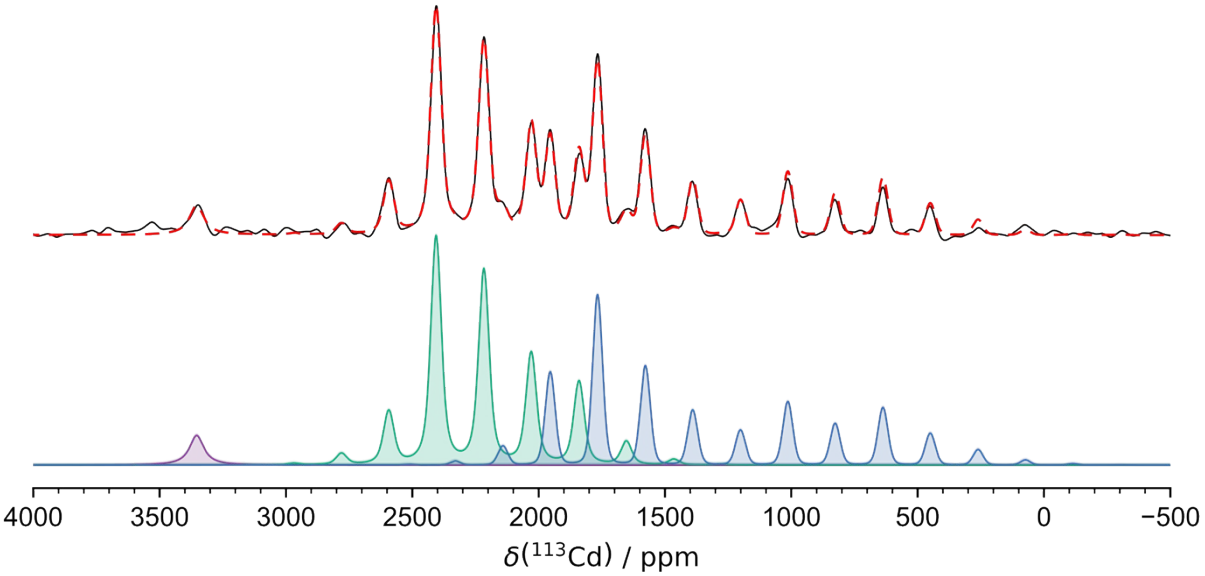

Figure S25 ^{113}Cd WCPMG-MAS NMR spectrum of YRh_2Cd_{20} recorded in 2048 scans with 80 echoes of which 12 were processed, each spanning 9 rotor periods at a MAS frequency of 12.5 kHz and 8.0 s recycle delay. The three shadings indicate the three crystallographically independent cadmium sites (see Tables 6 and S1).

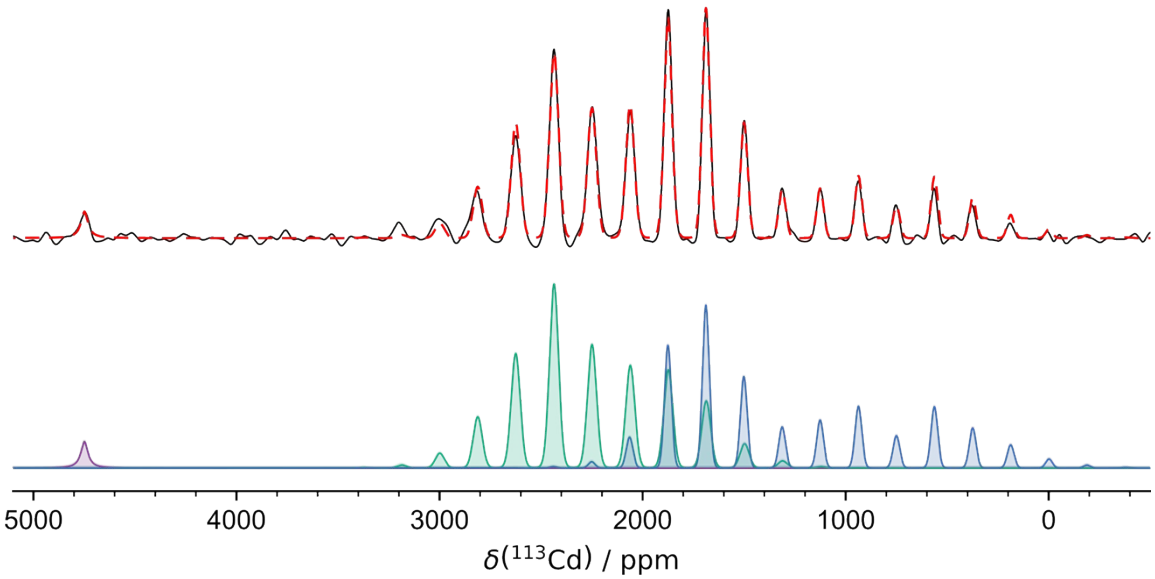

Figure S26 ^{113}Cd WCPMG-MAS NMR spectrum of $LaRh_2Cd_{20}$ recorded in 8192 scans with 80 echoes of which 12 were processed, each spanning 7 rotor periods at a MAS frequency of 12.5 kHz and 8.0 s recycle delay. The three shadings indicate the three crystallographically independent cadmium sites (see Tables 6 and S1).

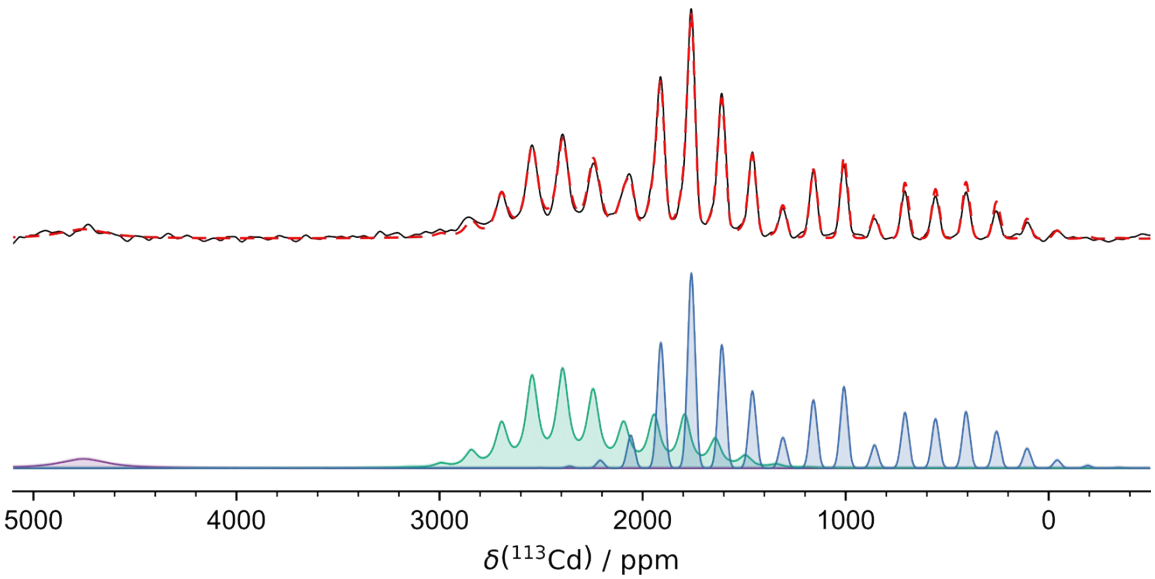

Figure S27 ^{113}Cd WCPMG-MAS NMR spectrum of $LaRh_2Cd_{20}$ recorded in 32768 scans with 80 echos of which 12 were processed, each spanning 7 rotor periods at a MAS frequency of 10.0 kHz and 8.0 s recycle delay. The three shadings indicate the three crystallographically independent cadmium sites (see Tables 6 and S1).

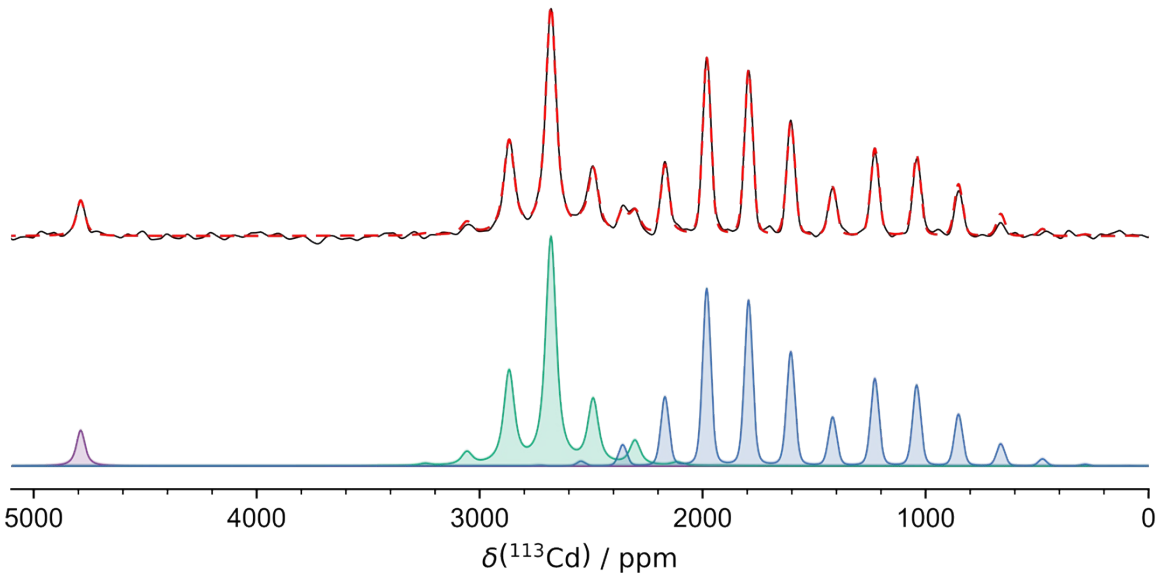

Figure S28 ^{113}Cd WCPMG-MAS NMR spectrum of $YbRh_2Cd_{20}$ recorded in 2048 scans with 80 echoes of which 10 were processed, each spanning 9 rotor periods at a MAS frequency of 12.5 kHz and 8.0 s recycle delay. The three shadings indicate the three crystallographically independent cadmium sites (see Tables 6 and S1).

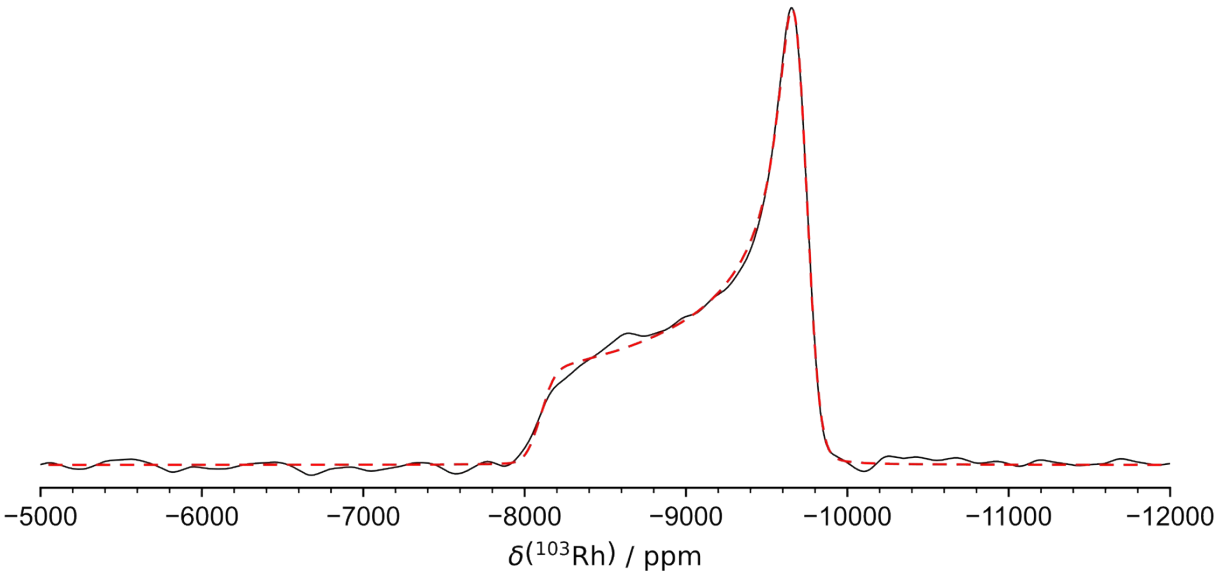

Figure S29 ^{103}Rh WCPMG NMR spectrum of YRh_2Cd_{20} recorded in 32768 scans with 80 echoes and 2.0 s recycle delay. The fit is shown as red dashed line.

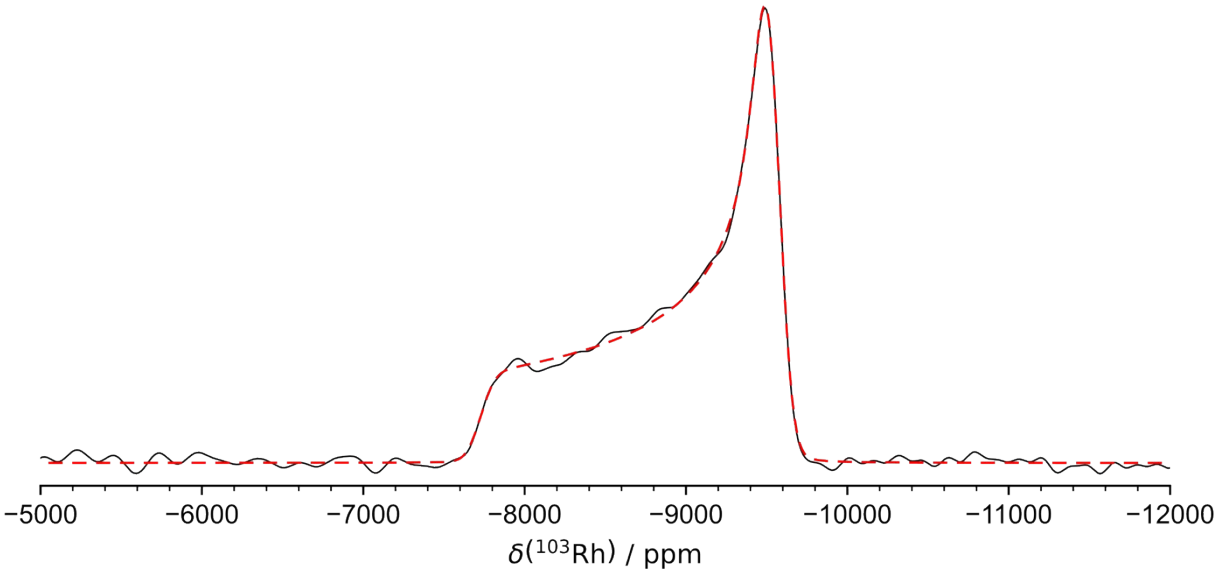

Figure S30 ^{103}Rh WCPMG NMR spectrum of $LaRh_2Cd_{20}$ recorded in 32768 scans with 80 echoes and 2.0 s recycle delay. The fit is shown as red dashed line.

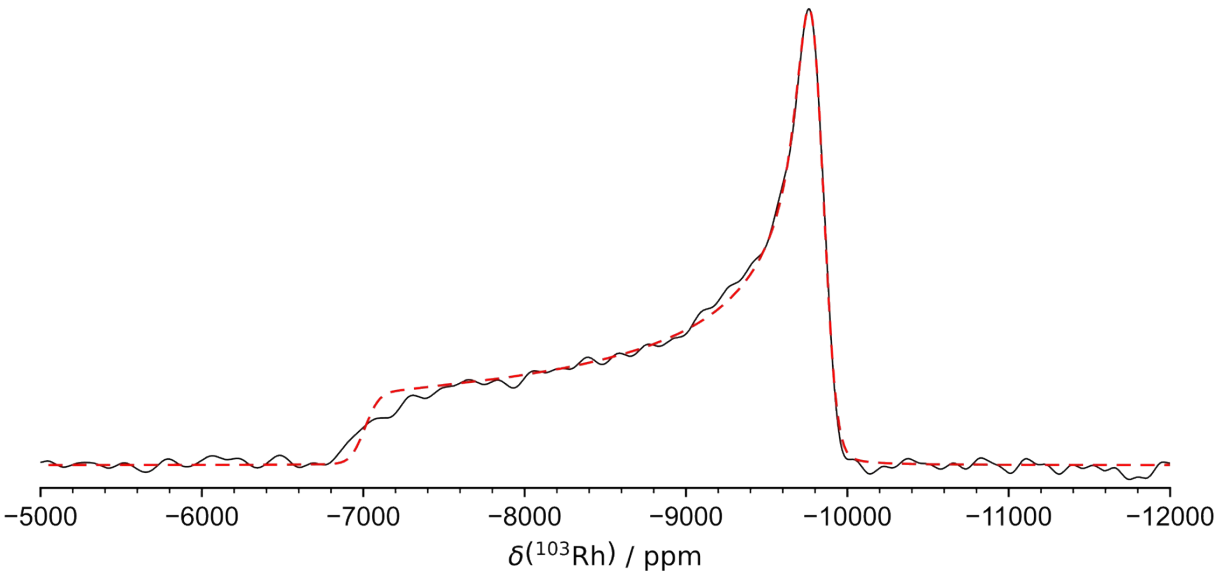

Figure S31 ^{103}Rh WCPMG NMR spectrum of $YbRh_2Cd_{20}$ recorded in 32768 scans with 80 echoes and 2.0 s recycle delay. The fit is shown as red dashed line.